Journal of Alloys and Compounds 488 (2009) 199–203

Contents lists available at ScienceDirect

Journal of Alloys and Compounds

journal homepage: www.elsevier.com/locate/jallcom

Effect of zinc substitution on structural and elastic properties of cobalt ferrite

V.G. Patil [a], Sagar E. Shirsath [b], S.D. More [c], S.J. Shukla [c], K.M. Jadhav [b,*]

[a] Department of Physics, ACS College Shankarnagar, Biloli, Nanded (M.S.), India
[b] Department of Physics, Dr. Babasaheb Ambedkar Marathwada University, Aurangabad 431004 (M.S.), India
[c] PG and Research Centre, Department of Physics, Deogiri College, Aurangabad 431004 (M.S.), India

ARTICLE INFO

Article history:
Received 13 July 2009
Received in revised form 7 August 2009
Accepted 10 August 2009
Available online 25 August 2009

PACS:
75.50.Gg
74.25.Ld
43.35.Cg

Keywords:
Ferrites
Structural properties
Elastic properties

ABSTRACT

Polycrystalline ferrites with general formula $Co_{1-x}Zn_xFe_2O_4$ ($x = 0, 0.2, 0.4, 0.6, 0.8$, and 1.0) were prepared by solid-state reaction technique. The structure and morphology of obtained products were investigated by X-ray diffraction (XRD) and scanning electron microscope (SEM) techniques. The analysis of XRD pattern revealed the formation of single-phase cubic spinel structure. Lattice constant increases with increase in zinc content, obeying Vegard's law. Elastic properties such as longitudinal velocity (V_l), transverse velocities (V_t), Poisson's ratio (σ) and Debye temperature (θ_D) have been studied. In the present work the elastic properties decreases with zinc composition x whereas Poisson's ratios almost remain constant. Debye temperature calculated from elastic data decreases with Zn substitution. A probable explanation has been proposed to explain the effect of zinc substitution on structural and elastic properties of cobalt ferrite.

1. Introduction

Ferrimagnetic cubic spinels namely ferrites possess properties of both magnetic materials and electric insulator. These properties make ferrites as an important material in many technological applications. These are preferred because of their high permeability in the radio frequency region, high electrical resistivity, mechanical hardness, chemical stability, etc. [1,2]. Their structural, electrical and magnetic properties depend on chemical composition, type and amount of dopant and method of preparation [3]. The structural and magnetic properties of spinel ferrite also depend on magnetic interaction and cation distribution in the two sub-lattices i.e. tetrahedral (A) and octahedral [B] site.

A study of the elastic behaviour of solids is of great importance in understanding the nature of inter-atomic and inter-ionic forces in solids. Zinc is a diamagnetic divalent ion which occupy essentially tetrahedral A-site when substituted in spinel ferrites. The important feature of cobalt ferrite is that it has a high magneto crystalline anisotropy and possesses a partial inverse spinel structure represented by $(Co_{0.1}Fe_{0.9})^A[Co_{0.9}Fe_{1.1}]^BO_4$. The substitution of zinc in cobalt ferrite is promising to manifest the structural and elastic properties. Physical properties such as density, molar volume, etc. manifest the structural changes. The study of elastic properties as a function of composition can be very useful in providing structural information of spinel ferrite. In the present work, we report our results on the structural and elastic properties of zinc substituted cobalt ferrite.

2. Experimental details

Polycrystalline specimens of $Co_{1-x}Zn_xFe_2O_4$ ($x = 0.0, 0.2, 0.4, 0.6, 0.8, 1.0$) were prepared by solid-state reaction, using analytical reagent grade oxides. Compounds were accurately weighed in molecular weight percentage with a single pan microbalance. The mixed powders were wet ground and pre-sintered at 900 °C for 12 h. The sintered powder is again re-ground and pelletized. Polyvinyl alcohol was used as a binder in making circular pellets of 10 mm diameter and 2–3 mm thickness. The pellets were finally sintered in muffle furnace for 1050 °C for 12 h and then slowly cooled to the room temperature.

The samples of cobalt–zinc ferrite were characterized by X-ray diffraction technique. The XRD patterns were recorded in 2θ range of 20–80° using Cu-K_α radiation at room temperature. Scanning electron microscope (SEM) technique is used to study the surface morphology and for the determination of particle size of the samples.

Ultrasonic velocity measurements were performed using McSkimin's pulse superposition method [4,5]. A pulse superposition technique has been employed using ultrasonic interferometer (Model SDU-1/003, System Dimension India). The error in the measurement of velocities is less than (±5 m/s). The bulk density of the specimens has been determined by hydro-static method.

The particle size of the samples was calculated using the relation:

$$t = \frac{0.9\lambda}{B \cos \theta_B} \quad (1)$$

where t is particle diameter, λ is wavelength of X-ray radiation, θ_B is Bragg's angle, β is full width at half maximum.

* Corresponding author. Tel.: +91 02402403384.
E-mail address: drkmjadhav@yahoo.com (K.M. Jadhav).

0925-8388/$ – see front matter © 2009 Elsevier B.V. All rights reserved.
doi:10.1016/j.jallcom.2009.08.078

The X-ray density was computed from the values of the lattice parameter using the formula [6]:

$$d_x = \frac{8M}{Na^3} \quad (2)$$

where 8 represents the number of molecules in a unit cell of spinel lattice. M is molecular weight, N is Avogadro's number, a is the lattice parameter.

The percentage porosity (P) of the samples was calculated using the formula:

$$P = 1 - \frac{\text{bulk density}}{\text{X-ray density}} \quad (3)$$

The distance between magnetic ions, hopping lengths in octahedral sites and tetrahedral sites is given by the following relation:

$$L_A = a\frac{\sqrt{3}}{4} \quad (4)$$

$$L_B = a\frac{\sqrt{2}}{4} \quad (5)$$

3. Results and discussion

3.1. Structural properties

The room temperature X-ray diffraction patterns of all the samples of $Co_{1-x}Zn_xFe_2O_4$ ferrite system are shown in Fig. 1. The inset of Fig. 1 shows the shift of one of the peaks (3 1 1) with Zn substitution. The XRD patterns show (2 2 0), (3 1 1), (4 0 0), (4 2 2), (3 3 3) and (4 4 0) planes, which belongs to f.c.c. cubic spinel structure. The XRD peaks are sharp and intense. It is also observed from XRD patterns that peak position slightly shifts towards lower angle, indicating the change in the inter-planar spacing (d) values.

The XRD data was used to determine lattice constant 'a', of all the samples of the $Co_{1-x}Zn_xFe_2O_4$. The lattice constant was calculated using inter-planar spacing (d) values and Miller indices ($h\,k\,l$) values, with an accuracy of ±0.002 Å. The values of lattice constant vary from 8.385 to 8.440 Å and are given in Table 1. It is observed that lattice constant 'a' increases linearly with zinc composition x. The variation of lattice constant of the present system can be explained on the basis of difference in ionic radii of the substituted ions. The ionic radii of Zn^{2+} (0.82 Å) [7] are larger than that of Co^{2+} (0.78 Å) [8] ions. In the present system Zn^{2+} ions are substituted in place of Co^{2+} ions and hence lattice constant increases with Zn content x. The variation of lattice constant with Zn substitution of the present system is similar in nature to the previous literature reports [9,10]. The increase in lattice constant with zinc substitution obeys the Vegard's law [11]. The uniform increase in lattice constant with zinc substitution indicates that lattice expands without disturbing the symmetry of lattice.

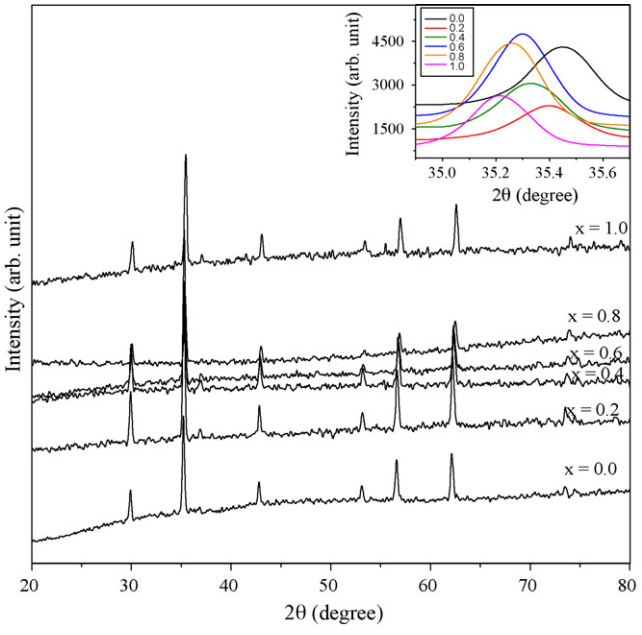

Fig. 1. XRD pattern of the ferrite system $Co_{1-x}Zn_xFe_2O_4$. Inset shows the shift in (3 1 1) peaks with 2θ.

Table 1
Lattice constant (a), particle size (t), bulk density (d), X-ray density (d_x), porosity (P), oxygen parameter (u) and theoretical lattice constant (a_{th}) of the Zn content x for $Co_{1-x}Zn_xFe_2O_4$.

Comp. x	0.0	0.2	0.4	0.6	0.8	1.0
a (Å)	8.387	8.4	8.412	8.421	8.431	8.441
t (μm)						
XRD	3.57	3.25	3.11	3.14	3	3.26
SEM	3.51	3.15	3.11	3.1	3.12	3.2
d (gm/cm^3)	4.864	4.878	4.89	4.9	4.924	4.935
d_x (gm/cm^3)	5.283	5.289	5.294	5.306	5.315	5.325
P (%)	7.94	7.76	7.64	7.45	7.35	7.15
u (Å)	0.387	0.389	0.391	0.394	0.396	0.398
a_{th} (Å)	8.389	8.386	8.384	8.381	8.378	8.375

The average crystalline size (t) of all the samples was obtained from the full width at half maxima of the most intense peak (3 1 1). The values of average particle size are presented in Table 1. The average particle size of all the samples is in between 3.0 and 3.57 μm.

The bulk density of the specimens has been determined by the hydro-static method. The values of the bulk density are given in Table 1. The bulk density was found to increase with Zn content x. In the present series the molecular weight of Co–Zn spinel ferrite increases with zinc substitution and volume of the unit cell also increases, but the rate of increase of molecular weight is more than that of volume. Therefore, the bulk density increases with zinc substitution in the present case.

The X-ray density was computed from the values of the lattice parameter using the relation (Eq. (2)). The values of X-ray density 'd_x' are given in Table 1. It can be seen from Table 1 that X-ray density increases with increasing zinc composition x. The increase in X-ray density can be related with the lattice constant. In the present series of Co–Zn spinel ferrites, the lattice constant increases with Zn^{2+} composition x. Due to increase in lattice constant, X-ray density should have been decreased, but in the present case molecular weight increases which overtake the increase in volume of the unit cell and hence X-ray density increases with Zn content x.

The percentage porosity 'P' of the sample was calculated using the values of X-ray density and bulk density. Table 1 gives the values of porosity as a function of zinc composition x. It is clear from table that density of the samples increases and the porosity decreases with increase in Zn composition x. The increase of the density is correlated with the atomic weight of the Zn^{2+} ions instead of Co^{2+} ions of lower density. The atomic weight of Zn and Co ions is 65.39 and 58.933 amu respectively. This is evidence of accelerated densification during the sintering process which led to reduction of porosity [12]. The low values of porosity indicate the highly dense structure of the prepared samples of Co–Zn spinel ferrite. The variation of bulk density and porosity with Zn composition x is depicted in Fig. 2.

The distance between magnetic ions at tetrahedral A (L_A) and octahedral B (L_B) sites was calculated using the relations (Eq. (4)) and (Eq. (5)). The variation of hopping length L_A and L_B is also shown in Fig. 3. Both L_A and L_B increases with Zn composition x. This may be attributed to the increase in lattice constant of the samples.

The bond length of tetrahedral (A) site 'd_{Ax}' (shortest distance between A-site cation and oxygen ion) and octahedral [B] site 'd_{Bx}' (shortest distance between B-site cation and oxygen ion), tetra-

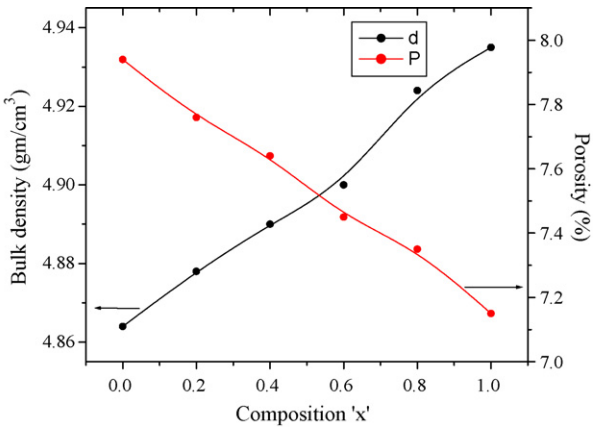

Fig. 2. Variation of bulk density and porosity with composition x for the system $Co_{1-x}Zn_xFe_2O_4$.

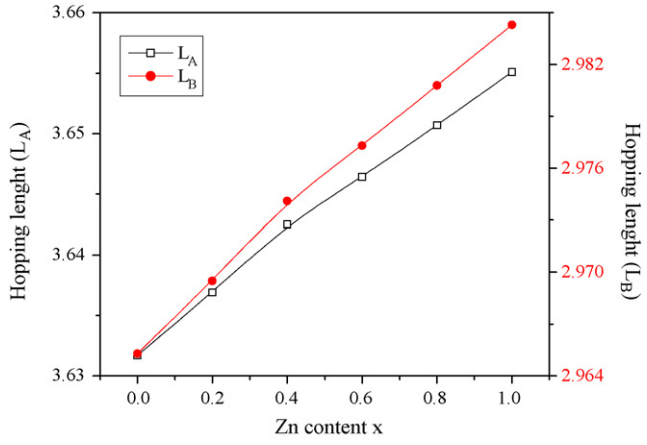

Fig. 3. Variation of hopping length (L_A and L_B) with composition x for the system $Co_{1-x}Zn_xFe_2O_4$.

hedral edge 'd_{AXE}', shared octahedral edge 'd_{BXE}' and unshared octahedral edge 'd_{BXEU}' can be calculated by putting the experimental values of lattice parameter 'a' and oxygen positional parameter 'u' of each sample using the equations reported by our group [13]. The values calculated from above mentioned equation are presented in Table 2. Table 2 indicates that the tetrahedral bond length d_{AX} and octahedral bond length d_{BX} increases as Zn^{2+} content 'x' increases. The tetrahedral edge 'd_{AXE}', unshared octahedral edge 'd_{BXEU}' does not vary much with composition while shared octahedral edge 'd_{BXE}' decreases. This could be related to the radius of Zn^{2+}, Co^{2+} and Fe^{3+} ions.

Using the cation distribution data the mean ionic radius of tetrahedral (A) site (r_A) and octahedral [B] site (r_B) was calculated. It is observed from Fig. 4 that r_A increases and r_B decreases with zinc substitution. The increase in r_A is due to the replacement of Fe^{3+}

Table 2
Tetrahedral bond (d_{Ax}), octahedral bond (d_{Bx}), tetra edge (d_{AxE}) and octaedge (d_{BxE}) (shared and non-shared) of $Co_{1-x}Zn_xFe_2O_4$.

x	d_{AX} (Å)	d_{BX} (Å)	Tetra edge (Å)	Octa edge d_{BXE} (Å)	
			d_{AXE}	Shared	unshared
0.0	1.903	2.042	3.108	2.823	2.967
0.2	1.906	2.052	3.112	2.827	2.971
0.4	1.909	2.054	3.117	2.831	2.976
0.6	1.911	2.059	3.120	2.834	2.979
0.8	1.913	2.01	3.124	2.838	2.983
1.0	1.915	2.064	3.128	2.841	2.986

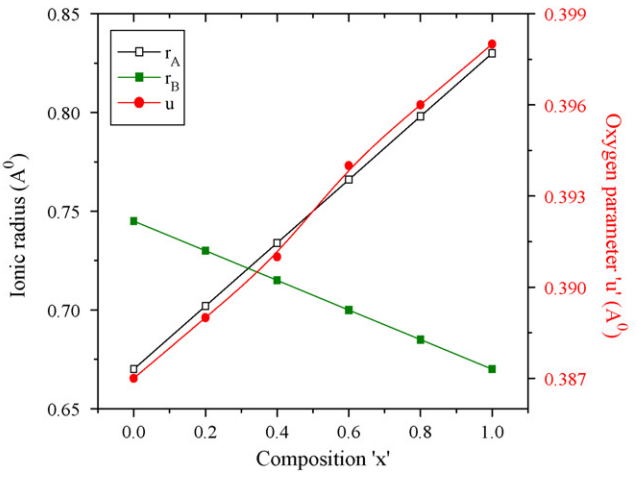

Fig. 4. Variation of ionic radius of the A-site (r_A) and of the B-site (r_B) and the oxygen parameter (u) for the system $Co_{1-x}Zn_xFe_2O_4$.

ions at the tetrahedral A-site by the larger radius Zn^{2+} ions. The decrease in r_B may be due to the increasingly migration of the larger Co^{2+} ions to the octahedral B-site instead of Fe^{3+} ions.

The oxygen parameter (u) can be calculated from the relation:

$$r_A = a_{th}\sqrt{3}\left(u - \frac{1}{4}\right) - R_0 \quad (6)$$

The obtained values of oxygen parameter (u) are given in Table 1. The relation between mean ionic radii r_A, r_B and oxygen positional parameter (u) as a function of zinc composition is shown in Fig. 4.

Theoretical lattice constant (a_{th}) can be calculated using the following relation:

$$a_{th} = \frac{8}{3\sqrt{3}}[(r_A + R_0) + \sqrt{3}(r_B + R_0)] \quad (7)$$

where r_A and r_B are the ionic radii of tetrahedral A and octahedral, B-site respectively.

R_0 is the oxygen parameter (1.32 Å).

The values of theoretical lattice constant are given in Table 1. It is seen from table that like observed lattice constant, theoretical lattice constant also increases. Further, it is observed that the theoretical and experimental lattice constant agrees reasonably well with each other suggesting that estimated cation distribution obtained by X-ray intensity ratio calculation is correct.

Fig. 5 depicts the scanning electron microscope images for typical samples (x = 0.2, 0.6 and 1.0). The average particle size was determined through SEM images and the values are presented in Table 1. It is observed from Table 1 that the particle size obtained from XRD data and SEM images is in good agreement with each other.

3.2. Elastic properties

The variation of the sound velocity longitudinal (V_l) and transverse (V_t) as a function of Zn composition x is depicted in Fig. 6. It can be seen from figure that both the velocity (V_l and V_t) decreases with substitution of Zn. The variation in molar volume with Zn composition is shown in Fig. 7. It is seen from figure that molar volume increases with Zn composition x.

The elastic moduli, Poisson's ratio (σ) and Debye temperature using the following relation:

$$\text{Longitudinal modulus}\,(L) = \rho v_l^2 \quad (8)$$

$$\text{Young's modulus}\,(Y) = 2(1+\sigma)G \quad (9)$$

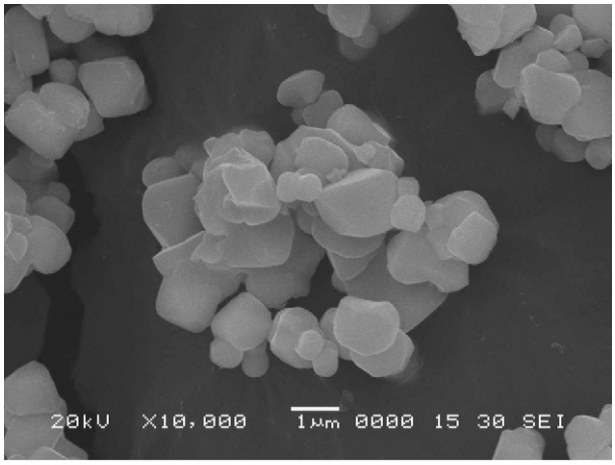

x = 0.2

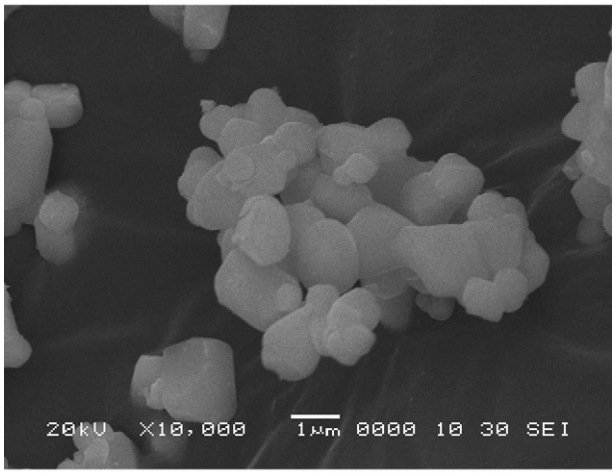

x = 0.6

Fig. 5. SEM images of typical samples (x = 0.2 and 0.6) for the system $Co_{1-x}Zn_xFe_2O_4$.

$$\text{Bulk modulus}\,(K) = L - \frac{4}{3}G \tag{10}$$

$$\text{Shear modulus}\,(G) = \rho v_t^2 \tag{11}$$

$$\text{Poisson's ratio}\,(\sigma) = \frac{L - 2G}{2(L - G)} \tag{12}$$

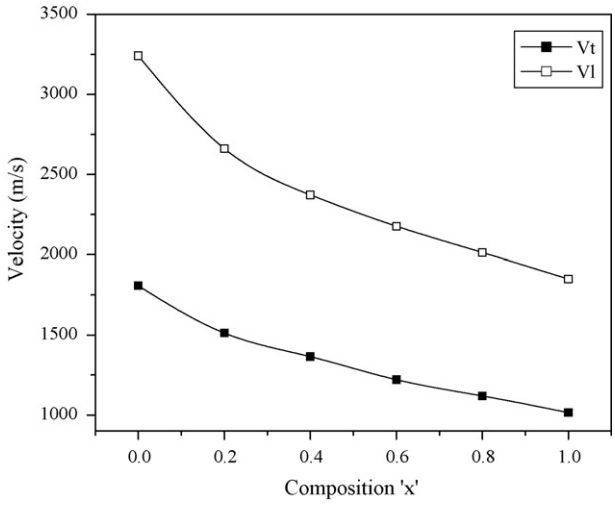

Fig. 6. Variation of sound velocity with composition x for the system $Co_{1-x}Zn_xFe_2O_4$.

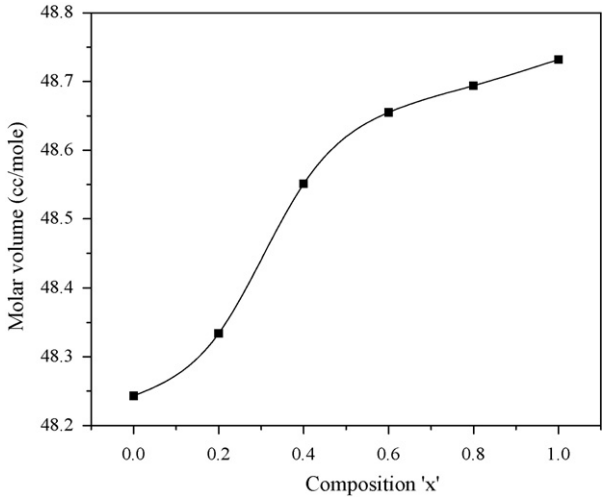

Fig. 7. Variation of molar volume with composition x for the system $Co_{1-x}Zn_xFe_2O_4$.

$$\text{Debye temperature}\,(\theta_D) = \frac{h}{k}\left[\frac{3\rho q N_A}{4\pi M}\right]^{1/3} V_m \tag{13}$$

where h is the Planck's constant, k is the Boltzmann's constant, M is the molecular weight and, q is number of atoms in the unit formula.

$$\frac{3}{\nu_m^3} = \frac{1}{\nu_1^3} = \frac{2}{\nu_t^3} \tag{14}$$

Since, the ferrites under investigation are porous the elastic moduli have been corrected to zero porosity using McKenzie's formula [14]. The corrected values of longitudinal modulus (L), Young's modulus (Y), bulk modulus (K) and shear modulus (G) are shown in Fig. 8. It can be observed from Fig. 8 that the values of longitudinal modulus, Young's modulus, bulk modulus and shear modulus decreases with zinc concentration x.

According to Wooster work [15] the behaviour elastic moduli is attributed to the strengthening of the inter-atomic binding between various atoms of the spinel lattice with increasing Zn ion content. The inter-atomic binding between various atoms is getting weakened continuously and therefore elastic moduli decreases with zinc content x.

Similar results have been observed in the case of Ni–Zn ferrites [16,17], wherein the inter-atomic binding between the various atoms decreases with increasing Zn content x [18]. It is significant

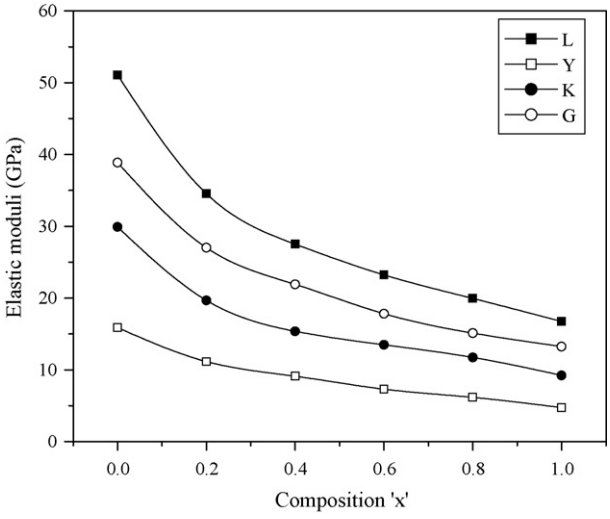

Fig. 8. Variation of elastic moduli with composition x for the system $Co_{1-x}Zn_xFe_2O_4$.

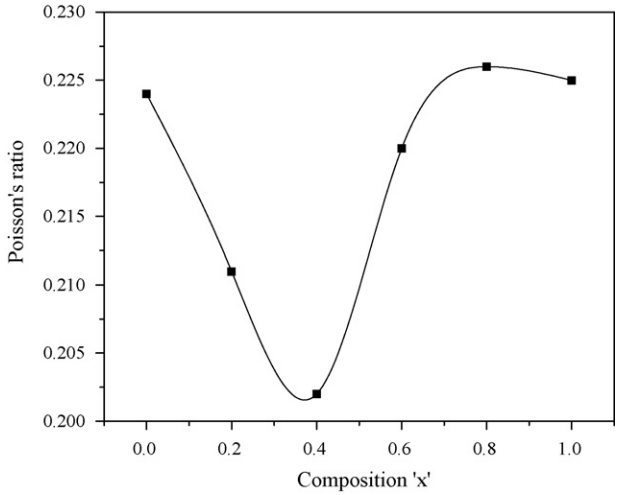

Fig. 9. Variation of Poisson's ratio with composition x for the system $Co_{1-x}Zn_xFe_2O_4$.

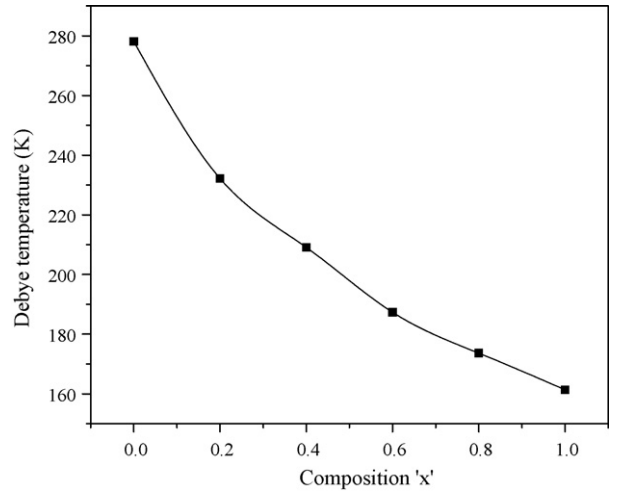

Fig. 10. Variation Debye temperature with composition x for the system $Co_{1-x}Zn_xFe_2O_4$.

to note that nonmagnetic substance when added in cobalt ferrite ($CoFe_2O_4$) that it has the same effect of weakening the binding strength. The Poisson's ratio (σ) shows nonlinear behaviour (Fig. 9). The value of σ is ranging from 0.202–0.226. These values are lying in the range from −1 to 0.5, which is in conformity with the theory of isotropic elasticity. Similar behaviour is observed in other Zn substituted ferrite [19,20].

The variation of Debye temperature (θ_D) is shown in Fig. 10. The Debye temperature decreases with Zn concentration x. The Debye temperature represent the temperature at which nearly all modes of vibration in solid are excited and decrease in Debye temperature implies the decrease in the rigidity of the ferrite.

4. Conclusions

The structural study of $Co_{1-x}Zn_xFe_2O_4$ spinel ferrite shows the effect of zinc substitution on the properties of cobalt ferrite. XRD patterns are sharp and intense and show the reflection which belongs to cubic spinel structure. The lattice constant increases with zinc substitution. The observed and calculated lattice constant are in good agreement with each other suggesting the estimated cation distribution is correct. X-ray density increases with zinc substitution. Bulk density increases whereas porosity decreases with Zn substitution. The elastic properties decreases with zinc composition x. Poisson's ratios shows nonlinear behaviour with Zn content x. Debye temperature decreases with Zn substitution.

Acknowledgments

One of the Author (VGP) is thankful Prof. R. V. Anavekar, Physics Department, Bangalore University, Banglore for providing ultrasonic data. He is also thankful to TIFR, Mumbai for providing XRD data.

References

[1] J.L. Dormann, D. Fiorani, Magnetic Properties of the Particles, 1992, North Holland, Amsterdam.
[2] S.E. Shirsath, B.G. Toksha, K.M. Jadhav, Mater. Chem. Phys. 117 (2009) 163.
[3] C.N.R. Rao, Chemical Approaches to the Synthesis of Inorganic Materials, Wiley Easter, New Age internationals New Delhi, 1993.
[4] I.H. Gul, A.Z. Abbasi, F. Amin, M. Anis-ur-Rehman, A. Masood, J. Magn. Magn. Mater. 311 (2007) 494.
[5] M.A. Ahmed, Phys. Stat. Sol. (A) 111 (1989) 567.
[6] R. Arulmurugan, G. Vaidyanathan, S. Sendhitnathan, B. Jeyadevan, J. Magn. Magn. Mater. 303 (2006) 131.
[7] M. Sertkol, Y. Köseoğlua, A. Baykal, H. Kavas, A. Bozkurt, M.S. Toprak, J. Alloys Compd., in press.
[8] R.C. Kambale, P.A. Shaikh, S.S. Kamble, Y.D. Kolekar, J. Alloys Compd. 478 (2009) 599.
[9] A. Lachebi, H. Abid, M. Driz, Y. Al-Douri, Int. J. Nano Mater. 1 (2008) 81.
[10] G.J. Baldha, K.G. Saija, K.B. Modi, H.H. Joshi, R.G. Kulkarni, Mater. Lett. 53 (2002) 233.
[11] B.D. Cullity, Elements of X-ray Diffraction, Reading, vol. 99, Addison-Wesley Publ. Comp. Inc., Massachusetts, 1956.
[12] A.K.M. Akther Hossain, S.T. Mahmud, M. Seki, T. Kawai, H. Tabata, J. Magn. Magn. Mater. 312 (2007) 210.
[13] S.S. Jadhav, S.E. Shirsath, B.G. Toksha, S.M. Patange, S.J. Shukla, K.M. Jadhav, Int. J. Mod. Phys. B, in press.
[14] J.K. McKenzie, Proc. Phys. Soc., London B 63 (1950) 2.
[15] W.R. Wooster, Rep. Prog. Phys. 16 (1953) 62.
[16] S. Srinivas Rao, D. Ravinder, Mater. Lett. 57 (2003) 3802.
[17] B. Revathi, T. Seshagiri Rao, J. Less Common Met 34 (1974) 91.
[18] S. Ramana Moorthy, B. Revathi, T. Seshagiri Rao, J. Less Common Met. 57 (1978) 29.
[19] D. Ravinder, K. Vijaya Kumar, B.S. Boyanov, Mater. Lett. 38 (1999) 22.
[20] M.K. Moinuddin, S. Ramana Murthy, J. Alloys Compd. 194 (1993) 105.